Supporting Information

for

Hepta-coordinated Ni(II) assemblies - structure and magnetic studies

Mateusz Reczyński[a], Mitsuru Akaki[b], Takamitsu Fukuda[c], Yuya Sawada[b], Kengo Nishii[b], Masayuki Hagiwara[b*], Wojciech Nitek[a], Barbara Sieklucka[a], Beata Nowicka[a,*]

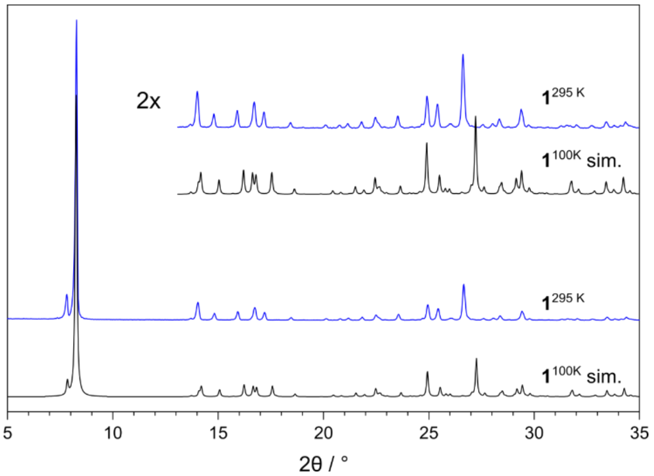

Figure S1. The PXRD pattern for **1** compared with the pattern simulated form SC data. A strong texture is observed with preferred (010) orientation for **1**, which was also taken into account for the simulated pattern (March-Dollase parameter = 0.6). The measurement temperatures are denoted in superscript.

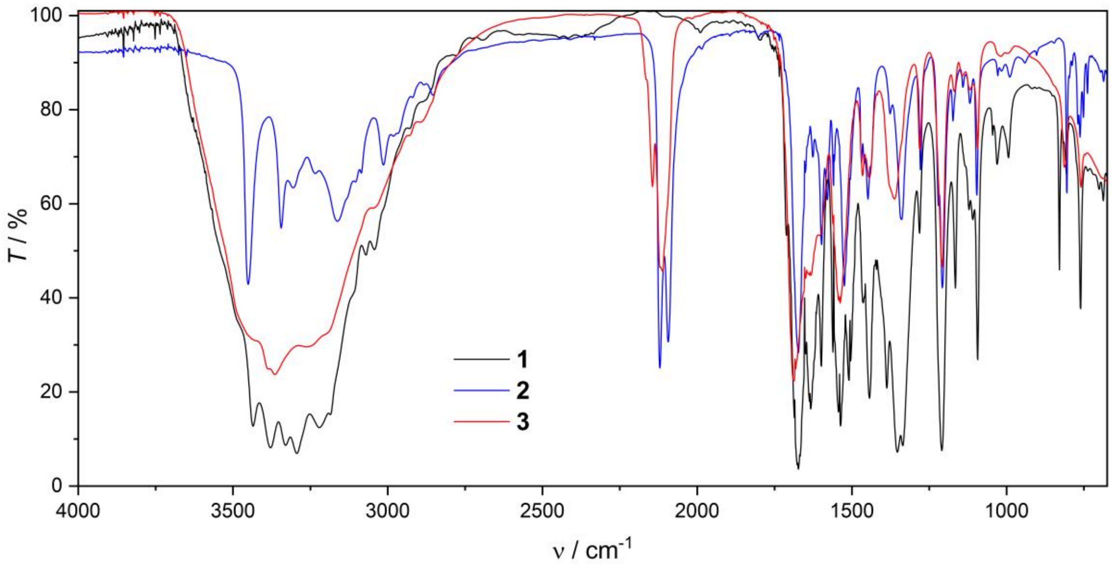

Figure S2. IR spectra for compounds **1**-**3**.

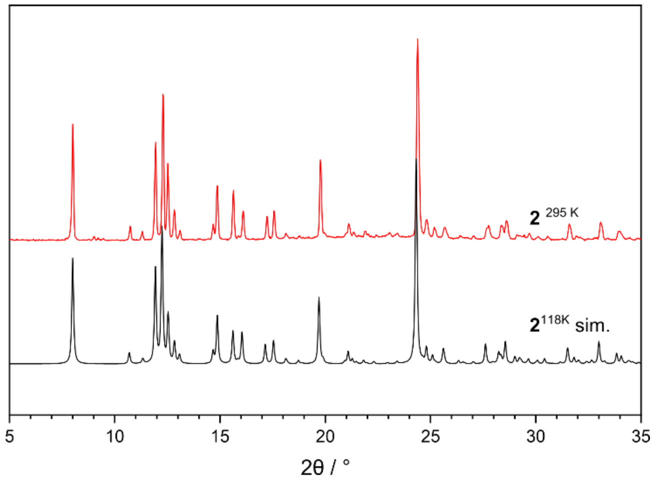

Figure S3. The PXRD pattern for **2** compared with the pattern simulated form SC data.

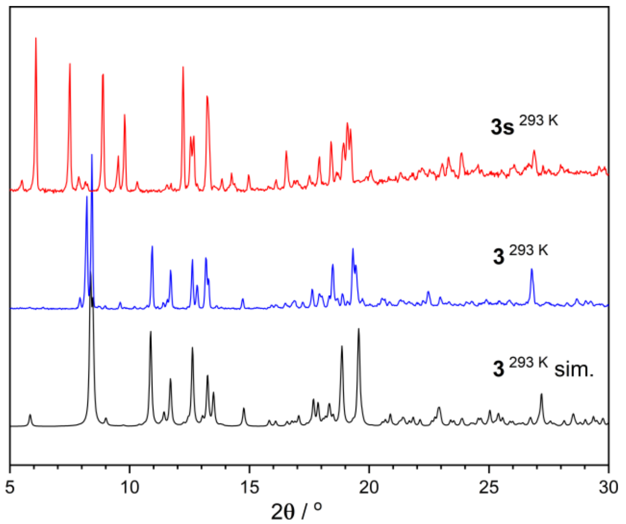

Figure S4. The experimental PXRD patterns for **3** and **3s** compared with the pattern for **3** simulated from SC data.

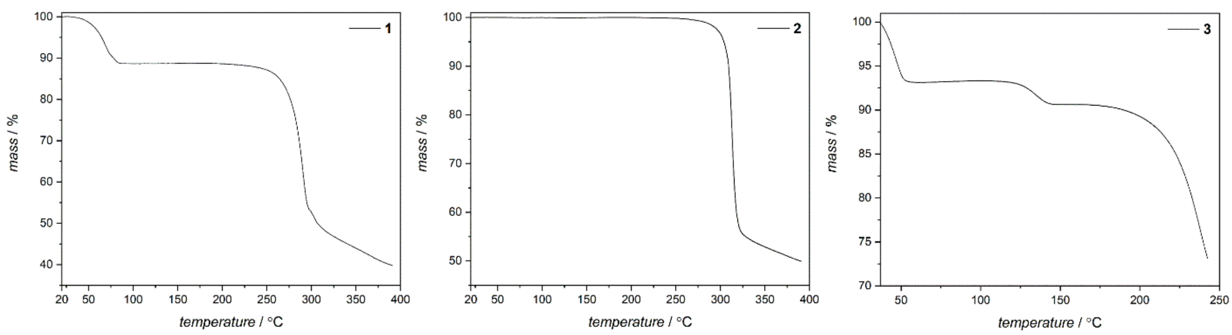

Figure S5. Thermogravimetric analysis for **1-3**.

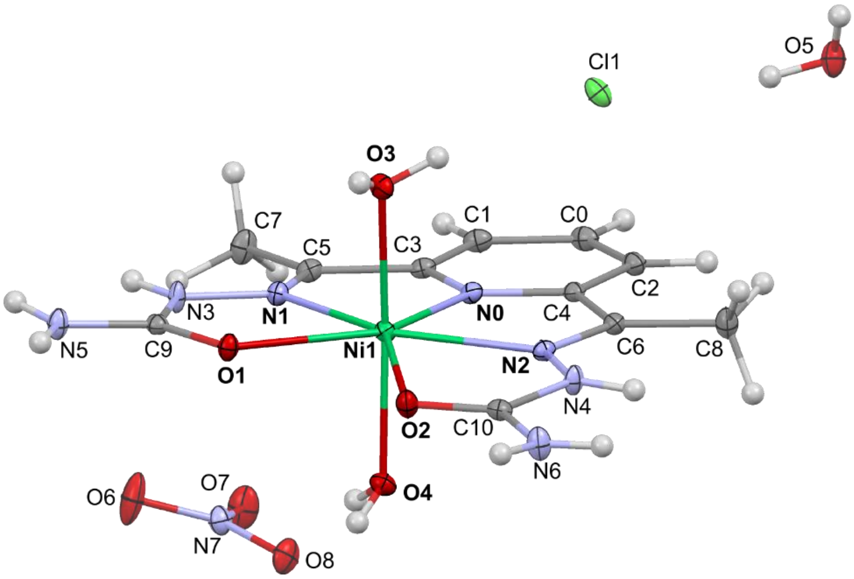

Figure S6. The asymmetric unit of **1**; ellipsoids at 50% probability.

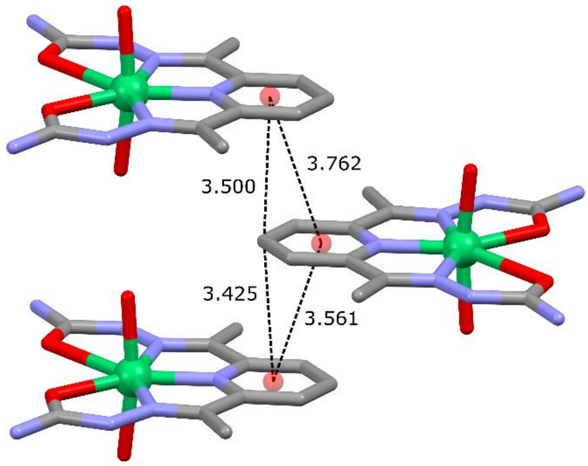

Figure S7. The π- π stacking in the structure of **1**.

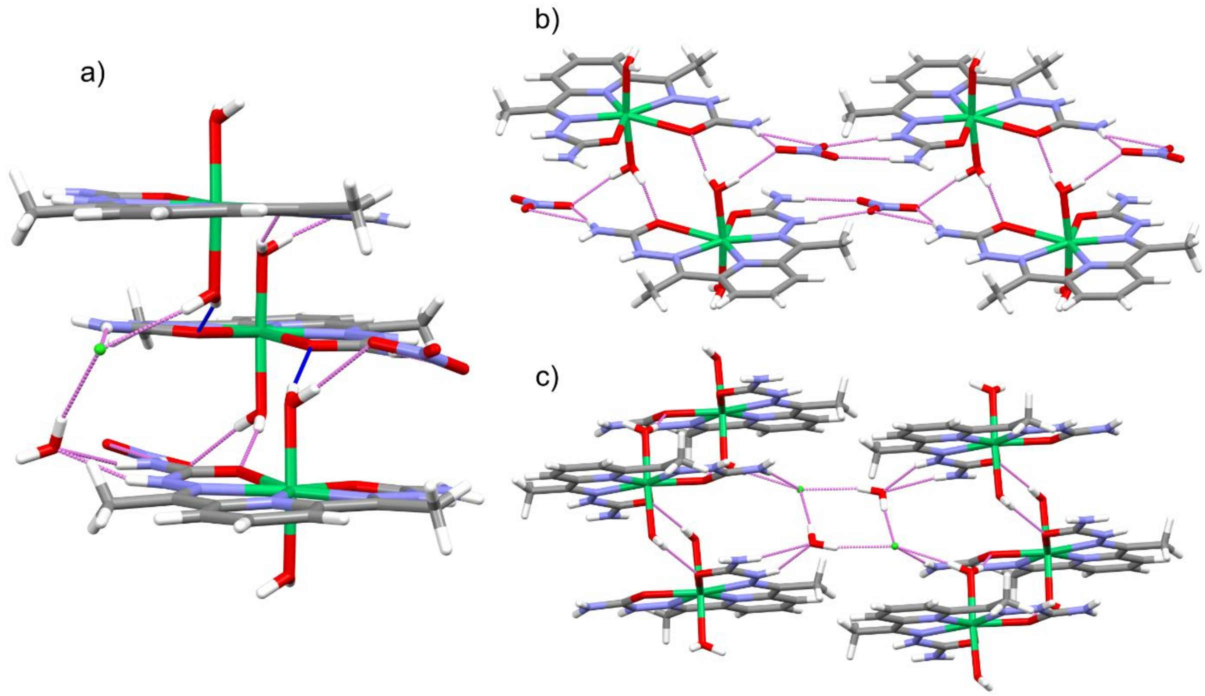

Figure S8. Hydrogen bonds in the structure of **1**: (a) direct interactions between the complexes (blue lines show the O-accepted H-bonds of the dapsc ligand); (b) H-bonds mediated by the NO_3^- anions; (c) H-bonds mediated by the Cl^- anions and water molecules.

Table S1. Hydrogen-bond geometry in **1**

D*—H···*A	***D*—H / Å**	**H···*A* / Å**	***D*···*A* / Å**	***D*—H···*A* / °**
N3—H3···O6^{ii}	0.81(2)	2.13(2)	2.9330(15)	174.5(18)
O3—H3*A*···O1^{v}	0.79(2)	2.05(2)	2.8192(13)	164(2)
O3—H3*B*···Cl1	0.82(2)	2.29(2)	3.1034(10)	170(2)
N4—H4···O5^{vi}	0.815(19)	2.038(19)	2.8006(16)	155.6(17)
O4—H4*A*···O8	0.82(2)	1.99(2)	2.7995(14)	173(2)
O4—H4*B*···O2^{vii}	0.81(2)	1.97(2)	2.7761(14)	169(2)
N5—H5*A*···O7^{ii}	0.83(2)	2.18(2)	3.0038(16)	175.2(18)
N5—H5*B*···Cl1^{v}	0.87(2)	2.40(2)	3.2519(12)	169.7(17)
N6—H6*A*···O6^{vii}	0.84(2)	2.521(19)	3.1025(16)	127.2(15)
N6—H6*A*···O8^{vii}	0.84(2)	2.30(2)	3.1358(16)	174.8(17)
N6—H6*B*···O5^{vi}	0.83(2)	2.30(2)	3.0109(16)	144.3(18)
O5—H1*WA*···Cl1	0.86(2)	2.27(2)	3.1132(11)	168(2)
O5—H1*WB*···Cl1^{viii}	0.80(3)	2.37(3)	3.1514(12)	167(2)

Symmetry codes: (i) −*x*+1, −*y*+1, −*z*; (ii) −*x*+1, −*y*+2, −*z*+1; (iii) -*x*, −*y*+1, −*z*; (iv) *x*−1, *y*, *z*; (v) −*x*+1, −*y*+1, −*z*+1; (vi) −*x*, −*y*, −*z*; (vii) −*x*, −*y*+1, −*z*+1; (viii) −*x*+1, −*y*, −*z*.

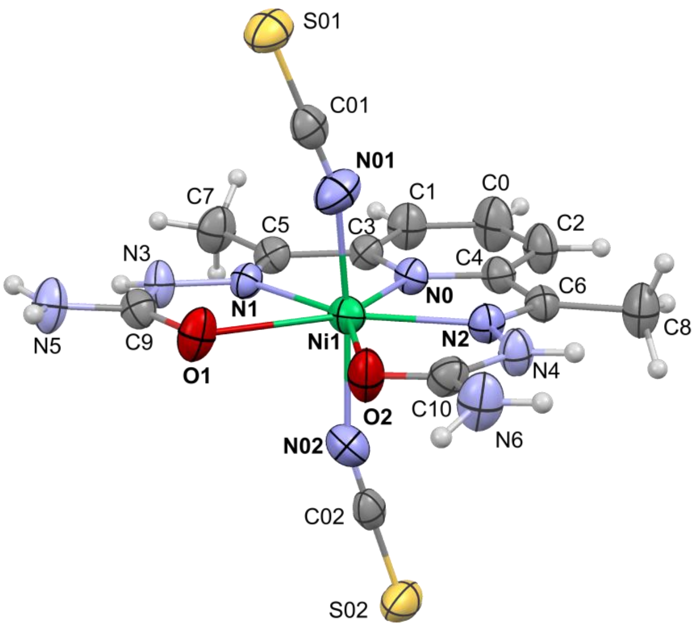

Figure S9. The asymmetric unit of **2**; ellipsoids at 50% probability.

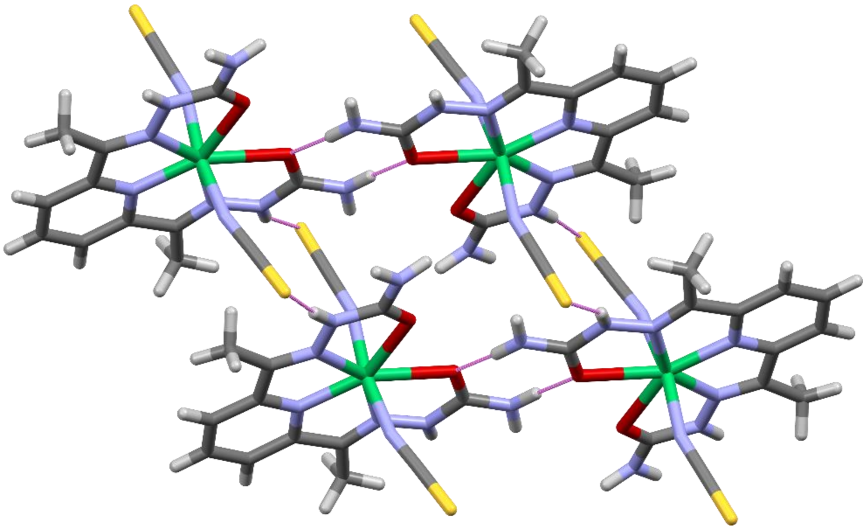

Figure S10. Hydrogen bonds in the structure of **2**.

Table S2. Hydrogen-bond geometry in **2**

D*—H···*A	***D*—H** / Å	**H···*A*** / Å	***D*···*A*** / Å	***D*—H···*A*** / °
N4—H4···S01^{ii}	0.87	2.5	3.343(3)	164
N3—H3···S02^{iii}	0.87	2.53	3.370(3)	163
N6—H6*A*···N02^{iv}	0.87	2.65	3.483(5)	160
N6—H6*B*···S01^{ii}	0.87	2.85	3.629(4)	150
N5—H5*A*···O1^{v}	0.87	2.13	2.966(4)	159
N5—H5*A*···O2^{v}	0.87	2.52	3.013(4)	116

Symmetry codes: (i) *x*, −*y*+1/2, *z*-1/2; (ii) *x*+1, *y*, *z*; (iii) *x*−1, *y*, *z*; (iv) −*x*+2, −*y*+1, −*z*+2; (v) −*x*+1,

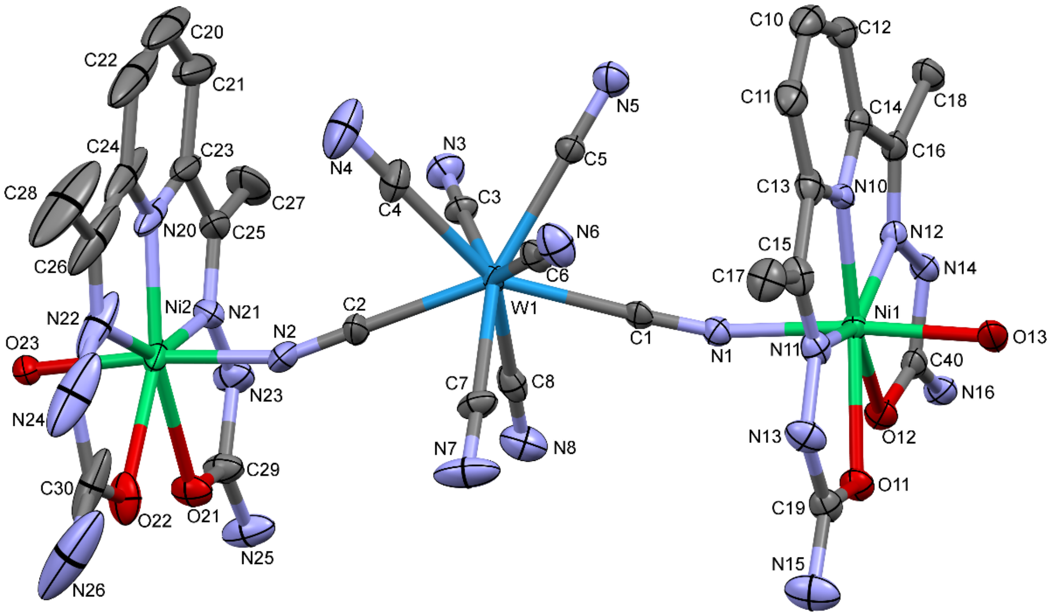

Figure S11. The asymmetric unit of **3**; H atoms and disordered water molecules omitted for clarity; ellipsoids at 50% probability.

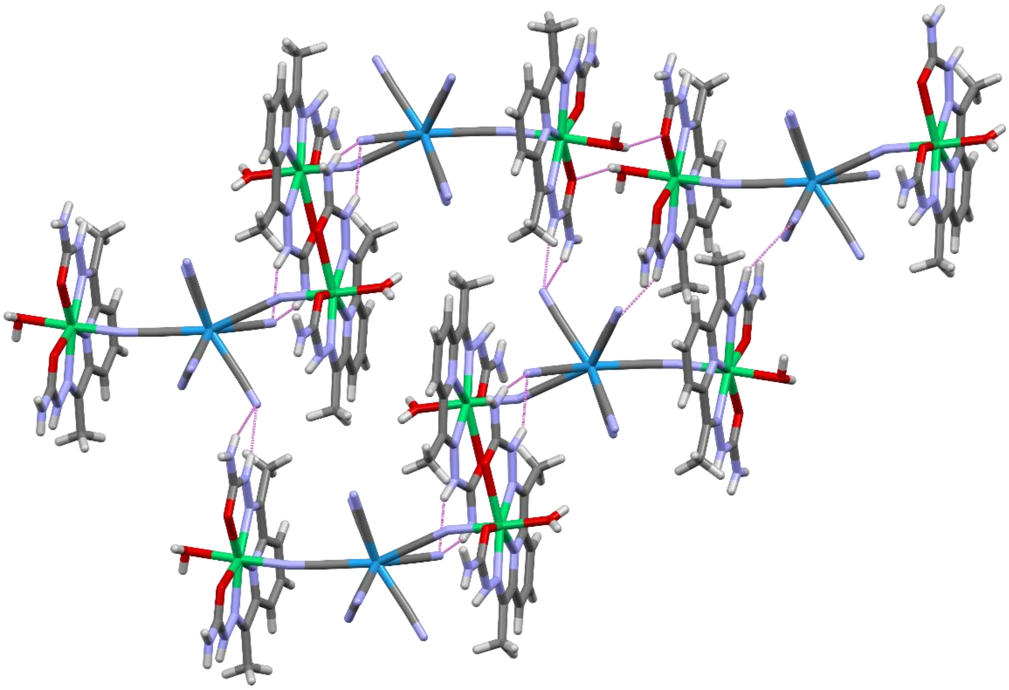

Figure S12. Direct hydrogen bonds linking trinuclear molecules in the (0 2 2) planes in the structure of **3**.

Table S3. Hydrogen-bond geometry in **3**

***D*—H**···*A*	***D*—H** / Å	**H···*A*** / Å	***D*···*A*** / Å	***D*—H···*A*** / °
N15—H15*A*···O7*W*	0.66	2.52	3.110 (8)	149
N15—H15*B*···N7^{iii}	0.86	2.39	3.154 (8)	149
N16—H16*A*···O1*W*^{i}	0.73	2.31	3.004 (6)	159
N16—H16*B*···N5^{i}	0.87	2.11	2.921 (6)	155
N25—H25*A*···N6^{iv}	0.77	2.49	3.162 (7)	146
N25—H25*B*···O1*W*^{v}	0.93	2.43	3.329 (6)	163
N25—H25*B*···O2*W*^{v}	0.93	2.59	3.271 (6)	131
N26—H26*A*···O6*W*^{v}	0.86	2.40	3.200 (13)	156
O13—H13*A*···O5*W*^{vi}	0.75	1.99	2.735 (6)	178
O13—H13*B*···O9*W*^{vi}	0.74	1.93	2.672 (5)	173
O23—H23*A*···N22	0.85	2.64	3.049 (6)	111
O23—H23*A*···O1*W*^{vii}	0.85	1.88	2.667 (5)	152
O23—H23*B*···O21^{viii}	0.73	2.08	2.770 (5)	157
O1*W*—H1*WA*···O4*W*	0.85	1.93	2.761 (6)	167
O1*W*—H1*WB*···O2*W*	0.86	1.95	2.718 (6)	149
O2*W*—H2*WA*···O11^{i}	0.78	2.06	2.802 (5)	159
O2*W*—H2*WA*···O12^{i}	0.78	2.49	3.002 (5)	125
O2*W*—H2*WB*···N7^{ix}	0.87	1.97	2.836 (7)	173
N13—H13···O7*W*	0.69 (7)	2.14 (8)	2.792 (7)	161 (8)
N14—H14···N5^{i}	0.92 (6)	2.22 (6)	3.025 (6)	145 (5)
N23—H23···N6^{iv}	0.85 (7)	2.04 (7)	2.845 (7)	159 (6)
N24—H24···N7^{ii}	0.81 (11)	2.63 (11)	3.318 (10)	144 (10)
N24—H24···O11*W*^{ii}	0.81 (11)	2.41 (11)	3.106 (10)	145 (10)

Symmetry codes: (i) −*x*, −*y*+1, −*z*; (ii) −*x*, −*y*, −*z*+1; (iii) −*x*, −*y*, −*z*; (iv) *x*−1, *y*, *z*; (v) *x*−1, *y*−1, *z*; (vi) −*x*+1, −*y*+1, −z; (vii) −*x*, −*y*+1, −*z*+1; (viii) −*x*−1, −*y*, −*z*+1; (ix) *x*, *y*+1, *z*.

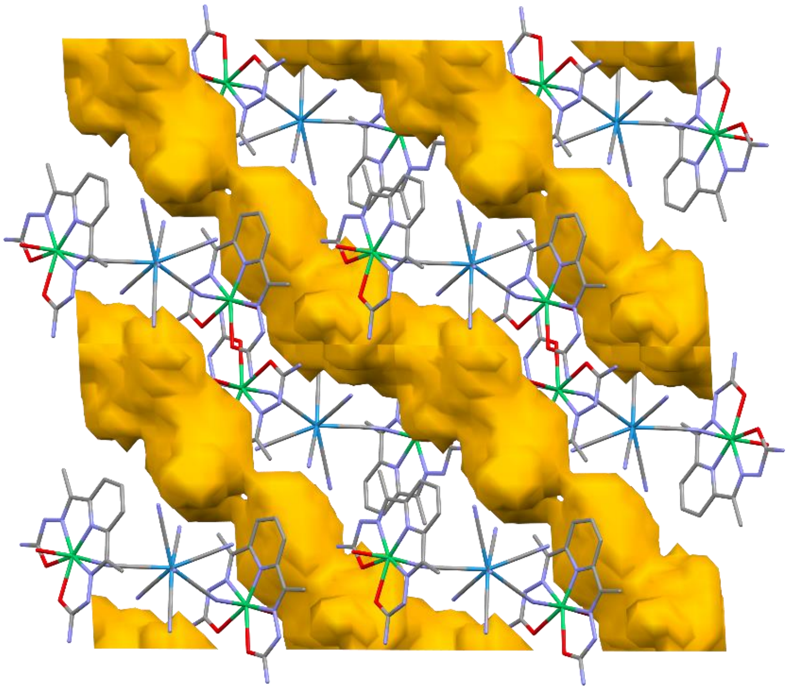

Figure S13. Channels filled with disordered crystallisation water in the structure of **3**.

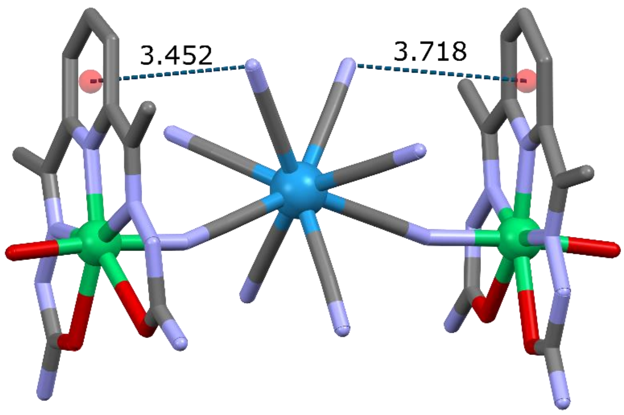

Figure S14. Close contacts between terminal CN ligands and pyridine rings of dapsc ligands in the structure of **3**.

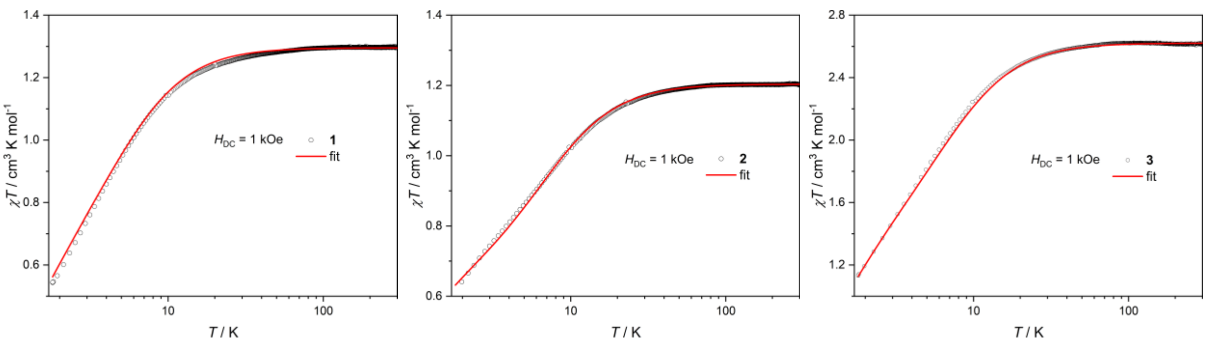

Figure S15. $\chi T(T)$ plots in logarithmic scale for compounds **1**-**3**.

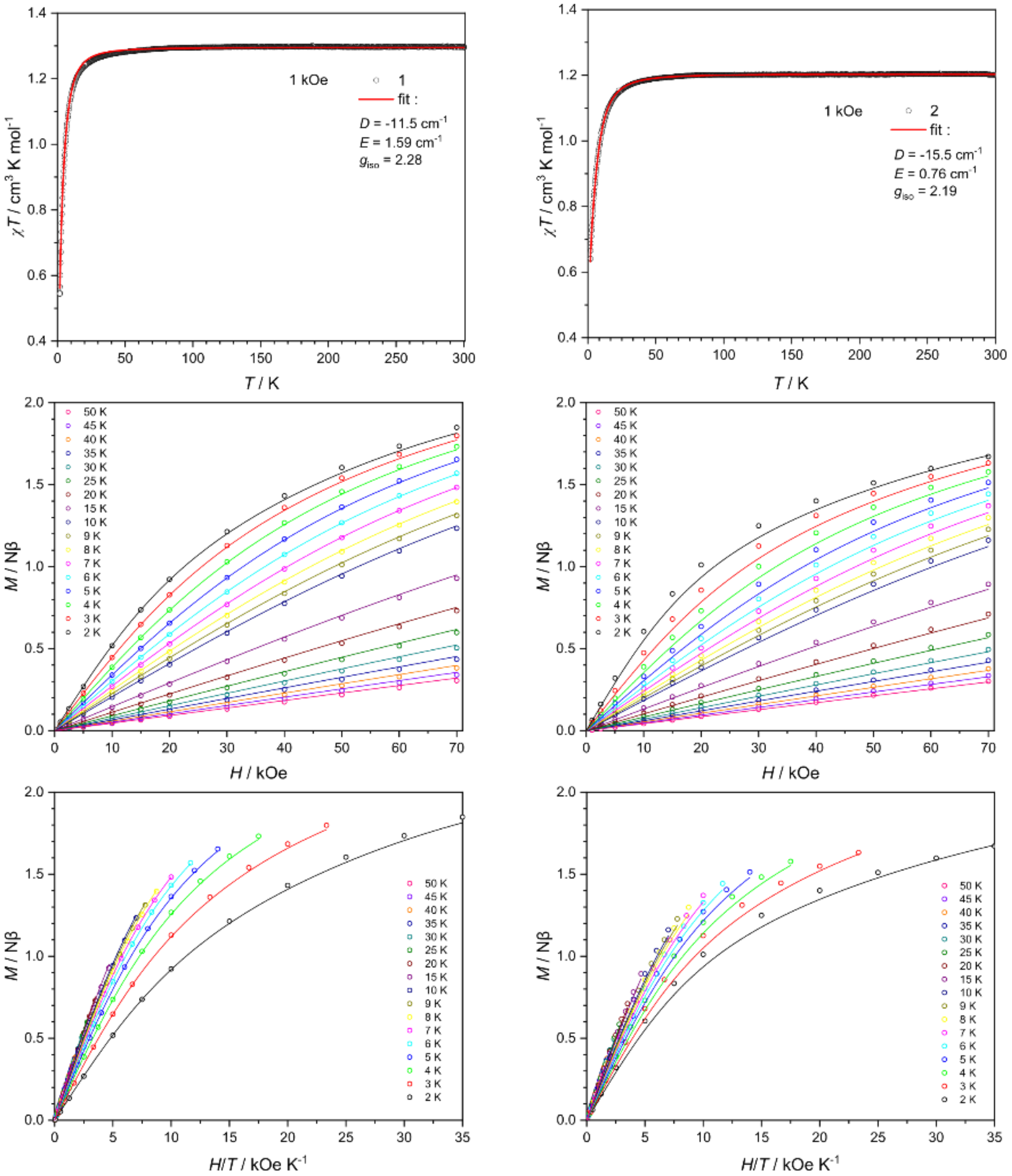

Figure S16. Concomitant fit of the $\chi T(T)$ (top), $M(H)$ (centre) and $M(HT^{-1})$ (bottom) curves for **1** (left) and **2** (right).

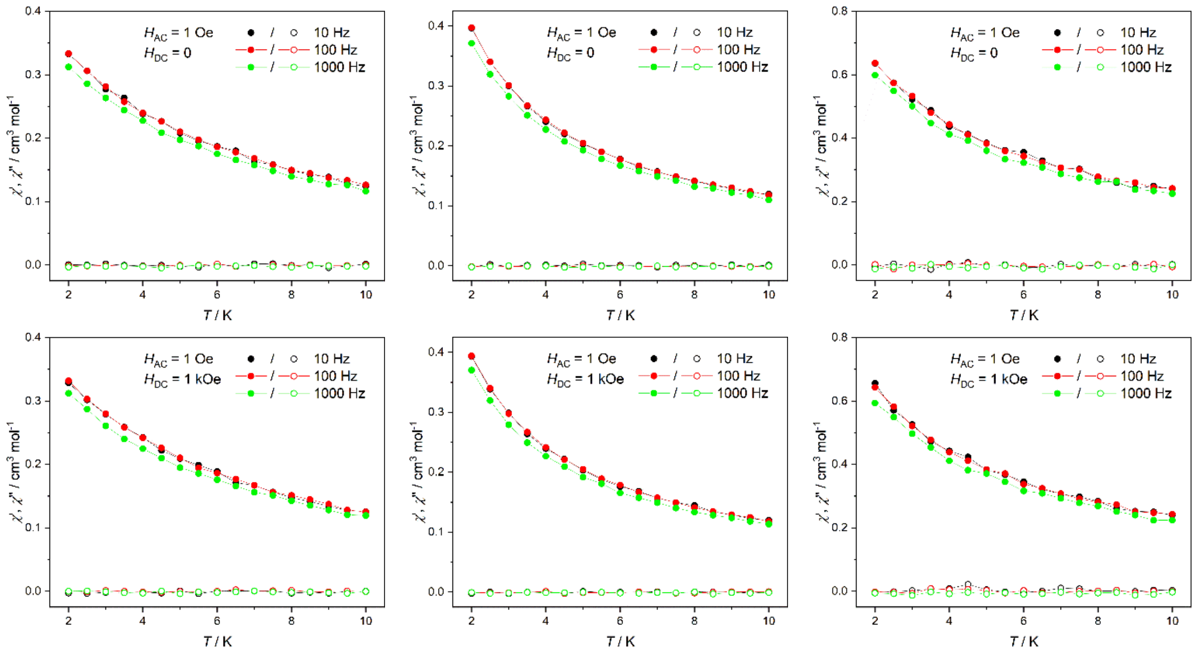

Figure S17. AC magnetic susceptibility in DC field 0 (top) and 1 kOe (bottom) for **1** (left), **2** (centre) and **3** (right); χ' - filled circles, χ'' - empty circles.

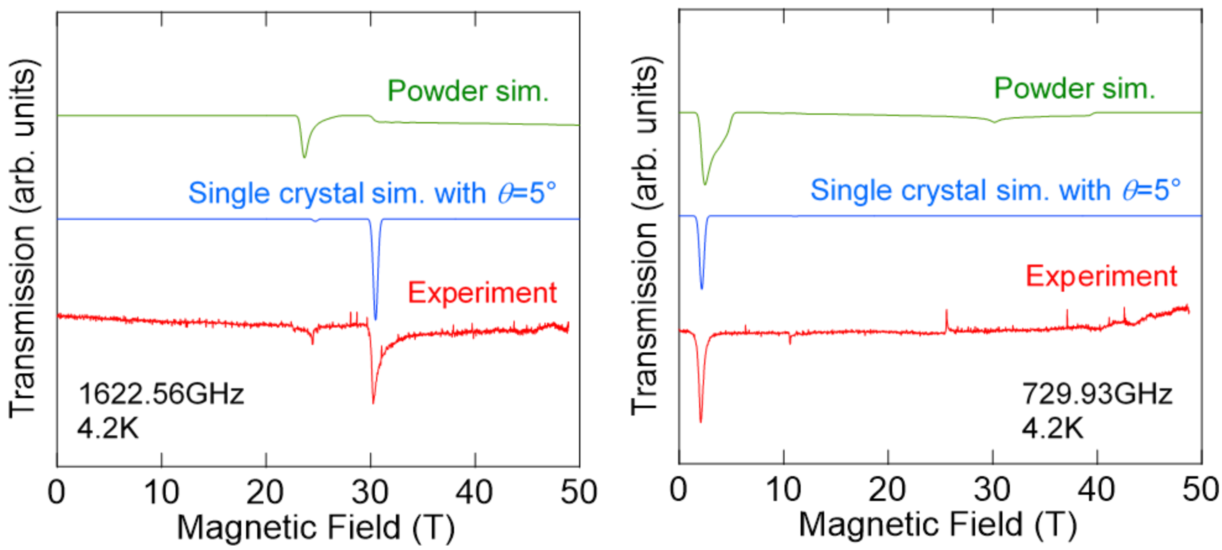

Figure S18. Simulation patterns of the EPR spectra at 4.2 K for the frequencies of 1622.56 GHz (left) and 729.93 GHz (right) corresponding to the spectra of **2**. The absorption width of 500 mT is used in each simulation. The upper and lower simulation patterns represent those for powder and single crystal with the deviation angle of the external magnetic field from the *z*-axis, θ=5°. The lowest line is the experimentally observed EPR spectra.

Table S4. ZFC parameters for **1**, **2** and **3** in comparison with literature data for related heptacoordinate Ni(II) complexes. Values obtained from magnetometric studies (*M*(*H*) fit or concomitant *M*(*H*) and $\chi T(T)$ fit) and/or **HF-EPR** (marked in blue bold print)

Reference	Compound	*D* / cm^{-1}	|*E*/*D*|	*g*
this work	[Ni(dapsc)(H_2O)$_2$]Cl(NO_3)·H_2O (**1**)	−11.5	0.14	2.275
		−10.5	**0.27**	
	[Ni(dapsc)(NCS)$_2$] (**2**)	−15.5	0.05	2.193
		−21.2	**0.10**	**2.14**
	[Ni(dapsc)(H_2O)]$_2$[W^{IV}(CN)$_8$]·11H_2O (**3**)	−15.4	0.09	2.290
		−15.0	**0.13**	**2.29**
19	[Ni(dapsc)(H_2O)$_2$](NO_3)$_2$·H_2O	−12.5	0.14	2.26
		−15.6	**0.12**	**2.23**
44	[Ni(dapsc)(NCS)$_2$]·2H_2O	−11.5	0.14	
44	[Ni(dapsc)(imidazole)$_2$](NO_3)$_2$·H_2O	−28.2	0.06	
20	[Ni(L^1)(H_2O)$_2$](NO_3)$_2$·H_2O	−13.9*	0.11	2.26
44	[Ni(L^1)(NCS)$_2$]·3H_2O	−12.4	0.12	
19	{[Ni(L^1)][Ni(CN)$_4$]}$_\infty$	−17.7	0.06	2.18
40	{[Ni(L^1)]$_3$[W^V(CN)$_8$](H_2O)$_2$}·2MeCN·12H_2O	−15		2.16
40	[Ni(L^2)(MeOH)(NO_3)](NO_3)	−12.5	0.09	2.22
40	{[Ni(L^2)]$_3$[W^V(CN)$_8$](H_2O)$_2$}·2MeCN·9H_2O	−5.0		2.17
41	[Ni(L^3)](ClO_4)$_2$·1.5CH_3NO_2	−17.2	0.076	2.165
42	[Ni(L^4)]·H2O	−8.5	0.19	2.20
43	[Ni(L^5)](ClO_4)$_2$	−12.8	0.136	2.181

L^1 and L^2 are dapsc derivatives with -NH_2 groups substituted by phenyl (L^1) or 4-biphenyl (L^2)

L^3 = 3,12-bis((1H-benzimidazol-2-yl)methyl)-6,9-dioxa-3,12,18-triazabicyclo[12.3.1]octadeca-1(18),14,16-triene)

L^4 = 3,12,18-triaza-6,9-dioxabicyclo[12.3.1]octadeca-1,14,16-triene-3,12-diacetic acid

L^5 = 3,12-bis(2-methylpyridine)-3,12,18-triaza-6,9-dioxabicyclo[12.3.1]octadeca-1,14,16-triene

* - values found consistent with HF-EPR results

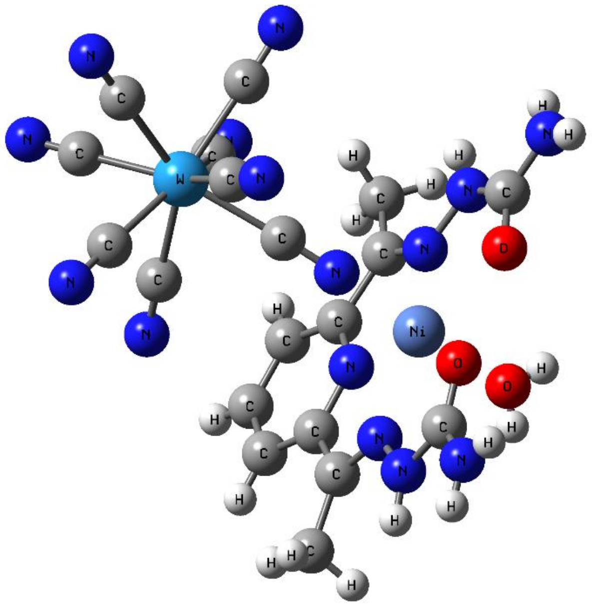

Figure S19. Coordination geometry used for the calculations of **3***.

Table S5. Spin Hamiltonian parameters at the CASSCF and NEVPT2 level *ab initio* calculations

compound		QDPT with CASSCF		QDPT with NEVPT2	
		2nd order SOC contribution	Effective Hamiltonian	2nd order SOC contribution	Effective Hamiltonian
1	D / cm^{-1}	−21.6	−19.4	−19.5	−17.8
	$\|E/D\|$	0.21	0.20	0.21	0.20
	g_x,	2.277		2.257	
	g_y	2.327		2.301	
	g_z	2.419		2.385	
	g_{iso}	2.341		2.315	
2	D / cm^{-1}	−41.5	−35.4	−37.9	−32.8
	$\|E/D\|$	0.04	0.03	0.04	0.03
	g_x,	2.279		2.261	
	g_y	2.296		2.276	
	g_z	2.514		2.477	
	g_{iso}	2.363		2.338	
3*	D / cm^{-1}	−25.0	−21.7	−22.4	−19.8
	$\|E/D\|$	0.09	0.09	0.09	0.08
	g_x,	2.273		2.254	
	g_y	2.297		2.275	
	g_z	2.424		2.391	
	g_{iso}	2.331		2.306	

Table S6. Wave functions for the ground and first excited states obtained at the QDPT with CASSCF level

compound	state #	energy / cm^{-1}	weight	spin	M_S
1	0	0.00	0.49	1	+1
			0.49	1	−1
	1	7.88	0.49	1	+1
			0.49	1	−1
	2	23.35	0.99	1	0
2	0	0.00	0.49	1	+1
			0.49	1	−1
	1	2.39	0.49	1	+1
			0.49	1	−1
	2	36.60	0.99	1	0
3*	0	0.00	0.49	1	+1
			0.49	1	−1
	1	3.75	0.49	1	+1
			0.49	1	−1
	2	23.60	0.99	1	0

Table S7. Wave functions for the ground and first excited states obtained at the QDPT with NEVPT2 level

compound	state #	energy / cm^{-1}	weight	spin	M_S
1	0	0.00	0.49	1	+1
			0.49	1	−1
	1	7.14	0.49	1	+1
			0.49	1	−1
	2	21.33	0.99	1	0
2	0	0.00	0.49	1	+1
			0.49	1	−1
	1	2.15	0.49	1	+1
			0.49	1	−1
	2	33.90	0.99	1	0
3*	0	0.00	0.49	1	+1
			0.49	1	−1
	1	3.28	0.49	1	+1
			0.49	1	−1
	2	21.42	0.99	1	0